3D3-3

Weighted Singular Unit Restoration in Interferograms Based on Complex-Valued MRF Model for Phase Unwrapping

Ryo YAMAKI [1], Akira HIROSE [2]
Department of Electronic Engineering, The University of Tokyo
7-3-1 Bunkyo-Ku, Tokyo, 113-8656,
[1] yamaki@eis.t.u-tokyo.ac.jp [2] ahirose@eis.t.u-tokyo.ac.jp

1. Introduction

Image filtering and phase unwrapping are the key techniques in generating digital elevation maps (DEMs) from obtained interferograms. In a usual case, the phase image that contains so many singular points (SPs) should be filtered and smoothed before being unwrapped. However, the filtering process smears dense fringes just perceptible in noisy interferograms.

Suksmono et al. proposed a method based on complex-valued Markov random field (CMRF) model for the estimation of the phase value of the pixel that corresponds to an SP [1]. In their method, they corrected a single pixel at the SP. However, an SP is a rotation, and determined by a set of four pixels [2] as described below. We name the pixel set the singular unit (SU). We have to correct all the four pixels in the SU for an effective restoration.

The authors therefore propose a new restoration algorithm, i.e., weighted singular unit restoration based on the CMRF model. In this method, the CMRF parameter is calculated as the weighted summation of the correlation vectors derived from the sample sites around the restoration target. The weighting factor is decided based on the distance between the sample site and the restoration target, and also on the number of the SPs included in the site. By using this restoration method, we succeed in generating a precise DEM. The delicate features which are lost in the usual filtering, are also preserved appropriately.

2. Restoration Based on Complex-Valued Markov Random Field Model

In the CMRF model, the probability $P(z_s)$ that a pixel value at s is z_s is derived from their neighbors. As shown in Fig.1, with the finite points included in the neighborhood (index : $t_1, t_2, \cdots$) around the point s, the probability is expressed as

$$P(z_s) = P(z_s|z_{t_1}, z_{t_2}, \cdots) \tag{1}$$

Therefore, we can estimate the most likely z_s value, $\hat{z}_s$ as the function of $(z_{t_1}, z_{t_2}, \cdots)$.

The calculation procedure for $\hat{z}_s$ is as follows. Here, we treat phase and amplitude as complex-valued entity, that is,

$$z(x, y) = a(x, y) \exp(\phi(x, y)) \tag{2}$$

where $a(x, y)$ is the amplitude (as the reliability of the data) and $\phi(x, y)$ is the phase value.

The correlation vector, $\mathbf{\Lambda}_{mn}$, among the target $z_{s_{mn}}$ and its neighbors

$$\mathbf{\Lambda}_{mn} = z_{s_{mn}} \boldsymbol{q}_s^* / (\boldsymbol{q}_s^* \cdot \boldsymbol{q}_s) \tag{3}$$

where $s_{mn} = \{s_{11}, s_{12}, s_{21}, s_{22}\}$ represents the pixels in the singular unit whose values are to be restored, which is shown in Fig.1. We also define $\boldsymbol{q}_s$ as the vector which is consisting of the values in the neighborhood around the singular unit as

$$\boldsymbol{q_s} = [z_{t_1} z_{t_2} \cdots z_{t_k}]^T \tag{4}$$

ISBN: 978-4-88552-223-9 C3055©IEICE

Let $[\cdot]^*$ and $[\cdots]^T$ be complex-conjugate transpose and simple transpose, respectively.

Figure 2 shows the positional relation of the SU, its neighborhood and the sample sites (at respective point p on the perimeter P) around them. When we find an SU, we can calculate the correlation vectors, $\mathbf{\Lambda}_{mn}(p)$, and the target $\mathbf{\Lambda}_{mn}$ as the weighted summation of the local $\mathbf{\Lambda}_{mn}$ as

$$\hat{\mathbf{\Lambda}}_{mn} = \sum_{p \in P} w(p) \mathbf{\Lambda}_{mn}(p) \tag{5}$$

where the normalized weights $w(\boldsymbol{p})$ are denoted as

$$w(p) = \frac{1}{r_p^2} \exp(-N_{st}(p)) \left[\sum_{p \in P} \frac{1}{r_p^2} \exp(-N_{st}(p)) \right]^{-1} \tag{6}$$

where r_p represents the distance between the center of the singular unit and the point p, and $N_{st}(p)$ is the number of the SPs included in the sample site around the point p. With the exponential term in (6), the influence of the SPs around the SU is reduced.

The target values can be estimated as

$$\hat{z}_{s_{mn}} = \hat{\mathbf{\Lambda}}_{mn} \boldsymbol{q}_s \tag{7}$$

3. Experimental Results

Figure 3(a) shows the original phase image (16-look averaged). Figure 3(b) shows the image filtered with the conically weighted window function whose radius is 3. Figure 3(c) shows the restored image by the proposed method (after 20 times iteration of the operation). In Fig.3(b), near the summit of the mountain and in the precipitous slope, the phase fringes are smeared and disappeared by the filtering operation. On the contrary, in Fig.3(c), the fringes are preserved and their topologies (the contours) seem more tractable. Figure 3(d),(e) and (f) show the distribution of the SPs in Fig.3(a),(b) and (c), respectively. The number of the SPs is 5095 in Fig.3(d), 681 in Fig.3(e), 134 in Fig.3(f), respectively. The adequate reduction in the number of the SPs shows the effectiveness of the proposed method. We also evaluated the height obtained from the phase data of Fig.3(b),(c) with phase unwrapping, scaling and bottom-raising compensation. Here we utilized so-called branch-cut method [3] which is the most fundamental unwrapping method.

The results are shown in Fig.4. Figure 4(a) and (b) show the DEMs calculated from the filtered phase image (Fig.3(b)) and the restored phase image with the proposed method (Fig.3(c)), respectively. In Fig.4(c) and (d), the elevation of Fig.4(a) and (b) are shown in gray scale. In Fig.4(a) and (c) (the conventional filtered image), we can recognize many unnatural branch-cuts especially near the summit of the mountain and also on the slope. On the contrary, in Fig.4(b) and (d), a natural and consistent landscape is reconstructed.

We have also evaluated mean squared error (MSE) and peak of squared error (PSE), which are calcurated with real terrain height data. We have also obtained the signal (squared height range (SHR)) to noise (MSE or PSE) ratios. The results are shown in Table 1. Because of the higher S/N in our method shown in Table 1, we can verify the effectiveness of the CMRF weighted singular unit restoration.

Table 1: MSE, PSE and SN ratio

Method	MSE		PSE	
	10^2[m^2]	$10 \log_{10} \frac{SHR}{MSE}$[dB]	10^4[m^2]	$10 \log_{10} \frac{SHR}{MSE}$[dB]
Weighted averaging filter	31.16	29.10	20.36	10.95
CMRF restoration	6.78	35.73	9.38	14.31

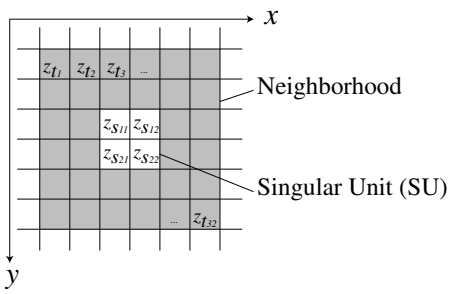

Figure 1: Restoration target (index : s_{mn}) and its neighbor pixels (index : $t_1, t_2, \cdots$)

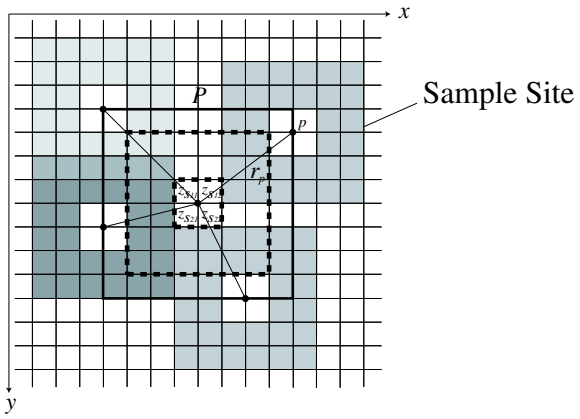

Figure 2: The weighted summation of the correlation vectors : $\mathbf{\Lambda}_{mn}$ on the perimeter around the singular unit and its neighborhood (indecated by broken lines)

4. Summary

The authors proposed a new restoration method, i.e., weighted singular unit restoration based on the CMRF model, and explained the restoration procedure. By using this restoration method, we succeed in generating a precise DEM where the delicate features are preserved appropriately. We have also validated our method by evaluating the errors between the real terrain height and the generated DEMs.

Acknowledgments

The authors would like to thank Dr. M. Shimada of EROC/JAXA, Japan, for supplying the InSAR data and the height data for evaluation.

References

[1] A. B. Suksmono and A. Hirose, ”Adaptive noise reduction of InSAR images based on a complex-valued MRF model and its application to phase unwrapping problem,” IEEE Transactions on Geoscience and Remote Sensing, Vol.40, No.3, pp.699-709, March 2002.

[2] A.Hirose K.Sugiyama, ”A radar system with phase-sensitive millimeter wave circuitry and complex-amplitude neural processing,” Int’l Conf. on Art. Neural Networks (ICANN)’98 Proc.2, 707-712 (Sept. 2-4, 1998, Skovde), Springer-Verlag.

[3] Dennis C. Ghiglia and Mark D. Pritt, ”Two-Dimensional Phase Unwrapping : Theory, Algorithms, and Software,” JOHN WILEY & SONS, INC., 1998.

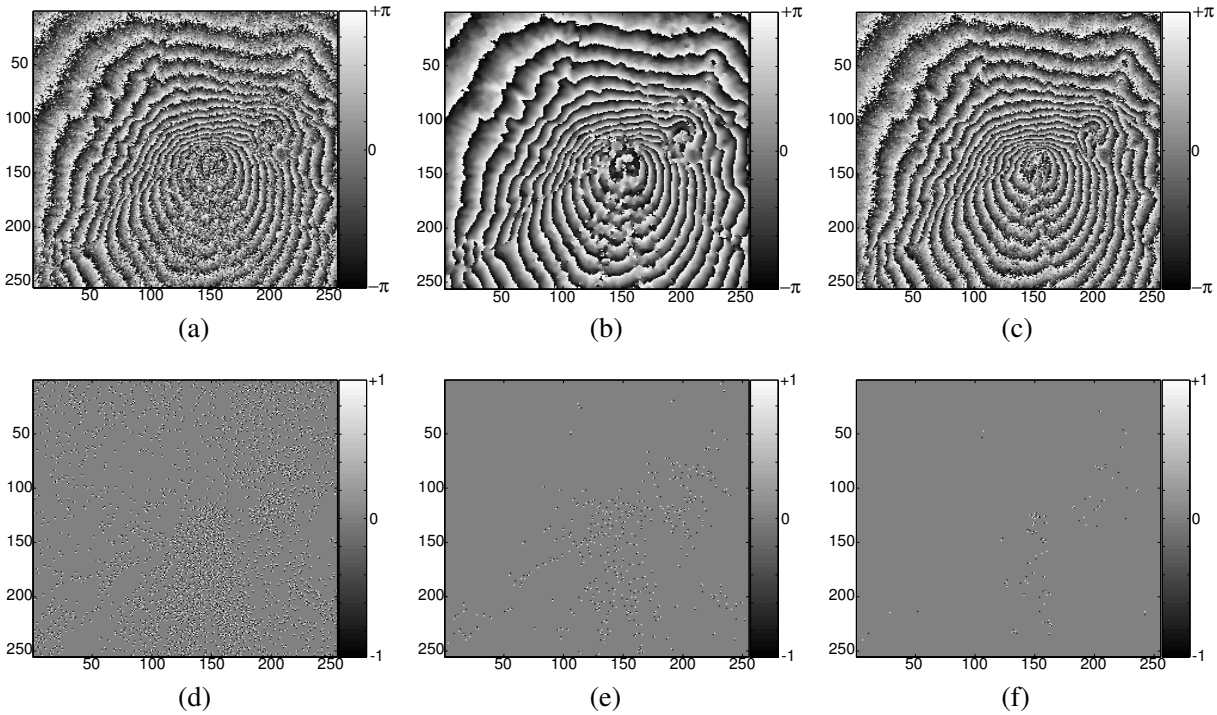

Figure 3: (a) Raw, (b) filtered and (c) restored phase images, and (d),(e) and (f) distribution of singular points in (a), (b) and (c), respectively.

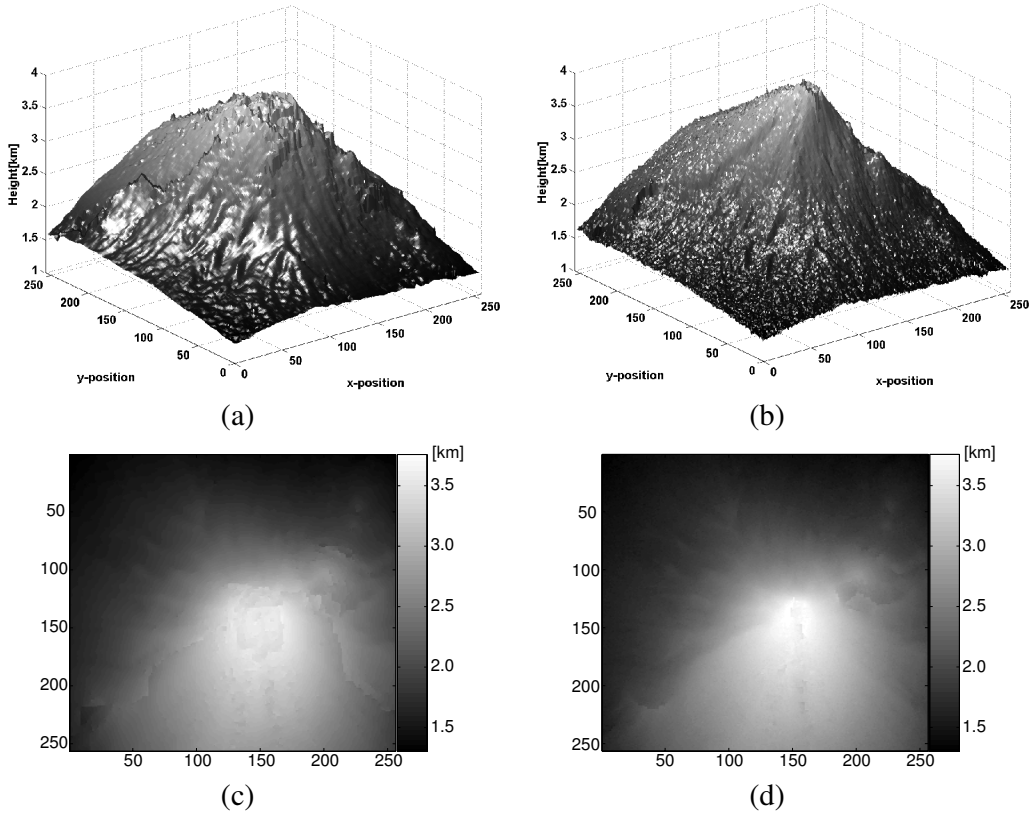

Figure 4: (a) DEM derived from conventionally filterd image (Fig.3(b)), (b) DEM derived from CMRF restored image (Fig.3(c)), (c) and (d) gray scale displays of (a) and (b), respectively.